Archives of Materials Science and Engineering

Volume 127
Issue 1
May 2024
Pages 12-22

International Scientific Journal
published monthly by the
World Academy of Materials
and Manufacturing Engineering

DOI: 10.5604/01.3001.0054.7283

Influence of L-PBF additive manufacturing parameters on the residual stresses and thermal distortions in AISI 316L stainless steel parts

M.O. Santos [a,b], G.F. Batalha [a,*], A. Farias [b], V. Seriacopi [b], E.C. Bordinassi [b], M. Adamiak [c]

[a] Department of Mechatronics and Mechanical System Engineering, Polytechnic School, University of São Paulo, Brazil
[b] Department of Mechanical Engineering, University Center of Maua Institute of Technology, São Caetano do Sul, Sao Paulo, Brazil
[c] Materials Research Laboratory, Faculty Mechanical Engineering, Silesian University of Technology, ul. Konarskiego 18a, 44-100 Gliwice, Poland
* Corresponding e-mail address: gfbatalh@usp.br, gfbatalha@gmail.com
ORCID identifier: https://orcid.org/0000-0001-8625-8499 (G.F.B.)

ABSTRACT

Purpose: The work aimed to numerically model through the Finite Element Method (FEM) the distribution of residual stresses and thermal distortions in parts generated by Laser Powder Bed Fusion (L-PBF) in stainless steel AISI 316L and validate the results obtained through experimental measurements on previously manufactured parts.

Design/methodology/approach: The design methodology followed a numerical approach through the Finite Element Method (FEM), the distribution of residual stresses and thermal distortions in parts generated by Selective Laser Powder Bed Fusion (L-PBF) in stainless steel AISI 316L and the FEM approach was validated trough the results obtained through experimental measurements on previously manufactured parts. The influence on three levels was verified through complete factorial planning of some manufacturing parameters, such as laser power, speed, and distance between scans (hatch), on the stress and distortion results of the samples and also on the samples simulated by FEM.

Findings: When results were compared about the average diameters, a relative error of less than 2.5% was observed. The average diameter was influenced by power and speed. Increasing power decreased the average diameter of the samples, while increasing speed and hatch increased the average diameter. When results are compared to measure the residual stresses, it is observed that the relative error was less than 1%. Power, speed, and the hatch itself influenced the residual stress. Increasing power increases residual stress while increasing speed and hatch decreases residual stress. The cooling rate and the transient thermal history are the control factors that influence the residual stresses and are directly related to the process parameters. The computational modelling followed by measurements and calibrations carried out in the experimental stages proved to be efficient and enabled the reproduction of thermal distortion and residual stresses with statistical confidence.

Research limitations/implications: Following the research, the aim is to evaluate the prediction of thermal distortions and residual stresses using the machine learning approach. Future research will study heating the building platform, which should also impact residual stresses.

Practical implications: Based on the results obtained in this research, it will be possible to select better additive manufacturing parameters for manufacturing 316L stainless steel parts. The parameters evaluated in the work were laser power, scanning speed, and hatch.

Originality/value: The innovation of the work lies in the robust simulation of the thermo-elastic behaviour of samples subjected to the additive manufacturing process, where it was possible to accurately relate the thermal distortions and residual stresses that appeared in the samples printed with the parts modelled by the FEM. The numerical-experimental validation makes it possible to extrapolate the studies to several other manufacturing parameters using only computational simulation and work with a more significant amount of data for a prediction study.

Keywords: Additive manufacturing, L-PBF, Stainless steel, 316L, Numerical simulation, Thermal distortions, Residual stresses

Reference to this paper should be given in the following way:

M.O. Santos, G.F. Batalha, A. Farias, V. Seriacopi, E.C. Bordinassi, M. Adamiak, Influence of L-PBF additive manufacturing parameters on the residual stresses and thermal distortions in AISI 316L stainless steel parts, Archives of Materials Science and Engineering 127/1 (2024) 12-22. DOI: https://doi.org/10.5604/01.3001.0054.7283

METHODOLOGY OF RESEARCH, ANALYSIS AND MODELLING

1. Introduction

Computers, one of the symbols of the third industrial revolution, have brought tremendous advances to traditional manufacturing methods. Automated systems such as computer numerical control (CNC) machining and robotic assembly lines significantly promote efficiency and consistency in fabrication methods; now, it is the time of the 4th industrial revolution, where additive manufacturing (AM) processes have outstanding progress [1-5]. Among the (AM) methods, also called 3D printing, it could be defined in a simple way as a "process of joining materials to make parts from 3D model data", usually layer upon layer [6]. It is becoming increasingly popular and has a constantly growing range of applications [7], providing unique opportunities for producing net shape geometries at the macroscale through microscale processing. Applications of additive technologies include biomedical, dental, automotive, aerospace, optics, and also textile and daily life sectors [3-11]. The AM process has disadvantages like poor surface roughness and residual stress. Tensile residual stress can negatively affect the performance of the pieces in service and cause geometry distortions [12]. The level of control presents inherent trade-offs necessitating the establishment of quality controls aimed at minimizing these undesirable properties [13], which is the most challenging of selective laser melting (SLM), also called powder bed fusion-laser (L-PBF). To control the issues, a proper understanding of the influence of process parameters on thermal distortion and residual stress profile during L-PBF is of paramount importance [14]. A significant problem associated with L-PBF components is the development of high internal residual stress [15] because of the repeated heating and cooling cycles. Successive layers of powdered raw material during the L-PBF construction process produce high cooling rates and high-temperature gradients associated with the process, resulting in residual stress buildup and thermal distortion in AM components. Parts may fail during L-PBF construction or later in service due to these high internal residual stresses. The localized melting and solidification cause residual stress during the process. As the laser melts the metal powder, it creates localized regions of high temperature that can cause thermal expansion and deformation. As the material solidifies and then cools, the different regions of the part cool at different rates, which can cause large strain misfits and internal stresses to form. The level and distribution of residual stress within a part can be influenced by various factors, including laser power, scanning speed, powder layer thickness, and part geometry [16], including the temperature control of the disk on which the part was manufactured. Thermal stresses occur when a volume cannot expand or contract without an obstacle in response to local changes in temperature, such as during laser radiation fusion. Materials in the liquid phase are not subject to thermal stresses. Thermal stresses occur from the temperature gradient or the solidification induction of the adjacent laser-melted areas in the solidified material. On the other hand, a decrease in thermal stress causes a decrease in residual stress [17]. Deformations of up to 0.2 mm in plates manufactured by SLM with a 1 mm thickness were found in [18]. The paper [19] also cites that residual stresses occur between the new layer and the manufactured feature when the new layer shrinks through consolidation upon the feature. Those stresses occur layer by

layer because the previous layer is already solid and preheated. According to [13], the thermal gradients present during building are affected by many process parameters (part size, build time, build plate/powder bed temperature, atmosphere, powder thermal characteristics, melt pool size, etc.). Aside from their potential impact on the mechanical performance and structural integrity of AM parts, residual stresses developed during processing may cause localized deformations, resulting in a loss of net shape, detachment from support structures, or failure of the AM part. Resolving residual stress and thermal distortion control in metal components through additive manufacturing (AM) is a significant challenge. To mitigate the challenge, the proper selection of AM process parameters is essential [20]. Although previous works indicate the importance of understanding the generation of residual stress and distortions in L-PBF processes, the underlying mechanisms for generating residual stress still need to be better understood. To better determine the factors that influence residual stress accumulation and prevent distortions, delamination, and fractures [21], a combination of parameters is sought for an ideal process window (one that meets product performance requirements). Therefore, L-PBF thermomechanical approach by finite element (FEM) simulation is potentially valuable, although they are a challenge due to the complexity of the physics involved in the process [22]. Numerical models can be used to predict the residual stress and deformation. The temperature distribution in the thermal models was applied as the load on the nodes, and stress and displacement fields were simulated [23]. According to [24], FEM analysis had been previously used to simulate the building process layer by layer and predict part distortions and residual stresses during the L-PBF process. In their study, [20] adopted both FEM simulation and experiment approaches to investigate the residual stress distribution in L-PBF 316L parts under realistic building conditions, with two levels of laser power and two laser scanning strategies. The typical L-PBF parameters for a real production scenario were adopted to reflect the realistic part building, and a sufficient number of layers were built. It was first adopted a FEM simulation model to investigate the effects of laser power and scanning path on the residual stress distribution.

The L-PBF experiment planning was carried out to obtain specimens, and an X-ray diffraction technique was adopted to measure the in-depth residual stress distributions. In the work of [25], the residual stress of the cast SS316L austenitic stainless-steel material was analyzed in detail by a cantilever model both experimentally and numerically. The average in-plane shrinkage stress in each additively deposited layer was determined directly from the distortion analysis of cantilever specimens and the proposed analytical formulation. A numerical finite element model (FEM) was developed to gain a better understanding of the residual stress state and was compared with experimental results. The purpose of the model, however, was not for prediction but for analysis of the residual stress field of the processed SS316L. In their study [26], the FEM-based simulations revealed the evolution of the melt pool and corresponding temperature distribution during the laser powder bed fusion (L-PBF) of 316L stainless steel samples. The maximum laser scanning speed resulted in 76-80 μm melt pool depth, 79-73 μm melt pool length, 77-93 μm melt pool width, and 1175-1335 °C temperature values. The paper [14] showed that residual stress was increased by increasing scanning speed and laser power and decreased by increasing hatch spacing. Cooling rate and transient thermal history are the controlling factors that significantly influence residual stresses. An increase in cooling rates by increasing both laser power and scanning speeds is one of many reasons for the identical behaviour. However, the influence is not the same magnitude for each processing parameter. Laser power is the most influential parameter, whereas hatch spacing leads to nominal variation in the residual stress [16]. A brief search of the previous publications confirms the complexity of achieving an accurate model to predict the residual stresses in additive-manufactured stainless steel parts printed by the L-PBF process [22,24,25, 27-56]. It is worth mentioning that the current research is still under development, so the authors are still carrying research about the influence of heat treatments on the L-PBF printed specimen; in this sense, results about the influence of the preheating of the building platform base as well as further post-heat treatment of the as-printed specimens will be addressed for a further publication.

Therefore, the present work aims to contribute to understanding how some process parameters such as laser power, scanning speed, and hatch affect the generation of residual stresses and distortions in the printed part of stainless steel 316L – both numerically (using the commercial software Simufact Additive from Hexagon MSC Software) and experimentally. A factorial design is used to select the variation of parameters. The statistical variance analysis method (ANOVA) was employed to correlate the results (residual stress and distortion) with the selected variables of the L-PBF process.

2. Materials and methods

2.1. Raw material and L-PBF equipment

The raw material was spherical particles of plasma-atomized austenitic stainless-steel powder, trademark PowderRange 316L, supplied by Carpenter Technology Corporation following the ASTM standard [57]. Figure 1 provides some information about the raw material used by the authors. Further information can be found on the material datasheet from the commercial supplier [58].

Stainless steel 316L samples were manufactured via LPBF additive manufacturing in an OMNITEK OmniSint-160 SLM equipment, ytterbium fibre laser module, and Rycus source nominal Power 500 W (see Fig. 2).

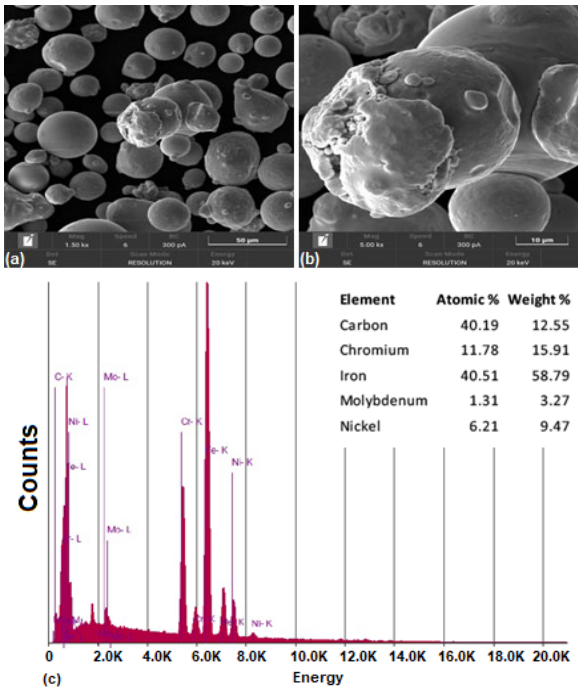

Fig. 1. Raw material characterization – plasma atomized 316-L atomized powder particle size and shape. (magnifications 1000 x (a) e 5000x (b), 300 pA - 20 keV

Fig. 2. OmniSint-160 additive manufacturing machine

Measurements of residual stresses of the 316L parts were carried out using the RIGAKU brand X-ray diffraction equipment, model Ultima IV (Fig. 3a), located at the Nuclear Research Institute (IPEN). The optical measuring equipment ATOS Core 80 – CP40/MV100 was used to measure the thermal distortions with a resolution of 5 Megapixels. Data was processed by the GOM Inspect 2021 software (Fig. 3b).

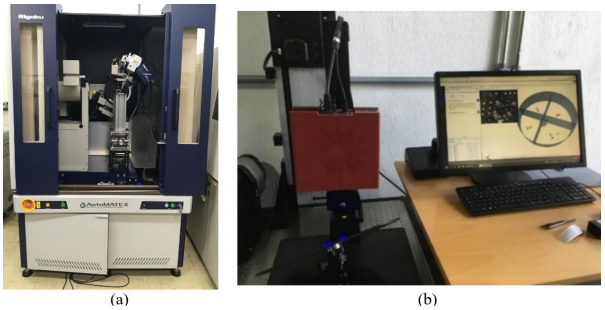

Fig. 3. (a) RIGAKU diffractometer, Ultima IV model, (b) GOM - ATOS Core 80 optical meter

2.2. Experimental methodology

To evaluate the impact of variations in the L-PBF manufacturing process parameters, such as the hatch distance, scanning speed, and laser power (as informed in Tab. 1), on the appearance of residual stresses and thermal distortions, 16 cylindrical specimens with 11.3 mm diameter and 10 mm height were used, according to a factorial design with the following variable factors.

Table 2 presents each manufactured part's test order and L-PBF parameters.

Table 1.
L-PBF mains process parameters

Power, W	100-200
Hatch distance, µm	50-90
Scanning speed, mm/s	500-1500

Table 2.
Manufacturing parameters experimental stage

Test order	Laser power, W	Scan speed, mm/s	Hatch, µm
1	150	1000	50
2	150	1000	90
3	100	1000	70
4	150	500	70
5	200	1000	70
6	150	1500	70
7	200	1500	70
8	150	1000	70
9	200	1500	50
10	100	1500	50
11	150	1000	70
12	200	1500	50
13	100	1500	90
14	100	500	90
15	200	500	90
16	100	500	50

Figure 4 shows 16 samples of stainless steel 316L printed on the printing base platform.

A wire EDM (electrical discharge machining) has enabled the specimens' extraction from the building platform using processing, significantly minimizing the residual stresses during cutting. A typical metallographic image from the specimen's top surface revealed porosity (Fig. 5); a further publication will address this disturbing effect on the model analysis.

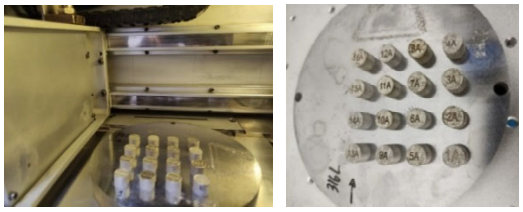

Fig. 4. As-printed LPBF 316L samples

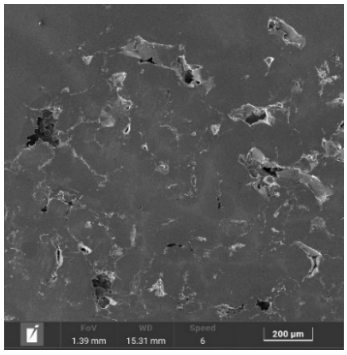

Fig. 5. Metallographic image of the 316L samples

2.3. Computational methodology

Numerical analysis was performed using the Simufact Additive 2020 FP1 software from Hexagon MSC Software, which uses CAD models to apply the same manufacturing conditions, defining a thermomechanical simulation. The authors have established the FEM settings directly by accessing a graphical user interface and the software calibration process. The calibration process consists of a preliminary step marked by defining the volume expansion factor (VEF). VEF is responsible for correcting the effects of thermal expansion and contraction since the element generated by the discretization of the domain in voxels (hexahedral finite elements – Fig. 6) consists of more than one material layer. For selecting such a factor, a cantilever geometry is often pre-selected, an option that facilitates characterising the state of deformations, strains, and stresses.

However, as such specifications would already be provided by the experimental study, convergence analysis of the factor was carried out for an arbitrary sample through the relationship with the data obtained numerically and experimentally – aiming at the approximation of the thermal distortions, so that if there is an equivalence in the displacements, it can be stated that the thermal deformation was correctly captured by the software and the residual stresses can thus be calculated, since they derive from deformations caused by the temperature gradient. When defining the metal powder melting process, the stages of the process were also defined, namely, construction of the part and separation of the base. The base separation was set up straight away. For the construction of the part, it was necessary to insert the constant parameters (the width of the laser beam and the scanning strategy) and variables for the study, namely laser power, scanning speed, and distance between scanning vectors (hatch) – the same parameters varied for the experimental part.

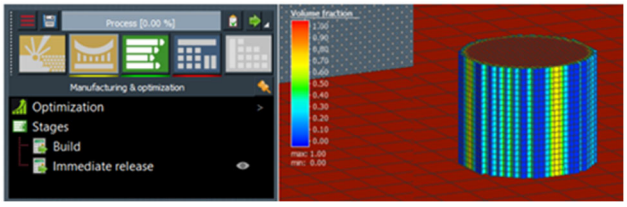

Fig. 6. Discretization of the geometry continuous domain

3. Results and discussion

3.1. Experimental thermal distortions

Initially, the sample (Fig. 7a) is subjected to scanning in the ATOS Core 80 equipment of its entire external surface Figure 7b, resulting in the geometry of Figure 7c, which is treated using the GOM Inspect software.

Fig. 7. a) 1A printed sample, b) optical measurement process, c) scanned geometry of the sample

After scanning each printed piece, the GOM Inspect software analyzes the metrological parameters. Initially, the geometry scanned by a cylinder is superimposed with the nominal dimensions of the part, which allows evaluation of the distortions resulting from the manufacturing process. For the research, only the mean diameter was defined as the distortion response parameter. Figure 8 shows a dimensional

comparison of the entire scanned surface of sample 1A about the nominal cylindrical body, with nominal dimensions of 10 mm height by 11.3 mm diameter. Warm colours indicate larger dimensions and cool colors indicate smaller dimensions than the nominal value.

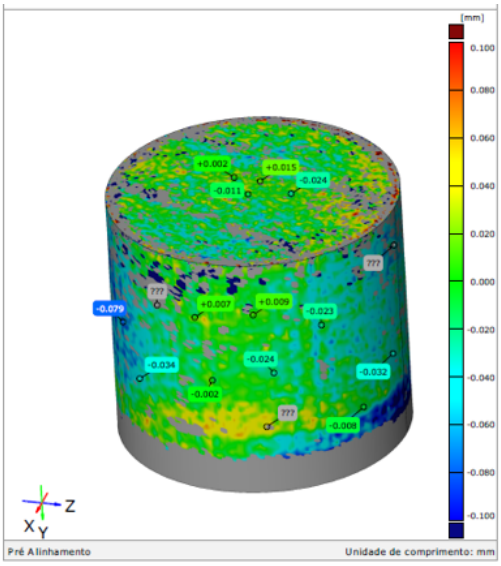

Fig. 8. Representation of distortions of the 1A sample

3.2. Experimental residual stresses

In the given step, the samples' residual stresses were measured. Measurements were taken on each piece's side. In Figures 9a and 9b, the part measured by the RIGAKU diffractometer, model Ultima IV, is visualized in the lateral position.

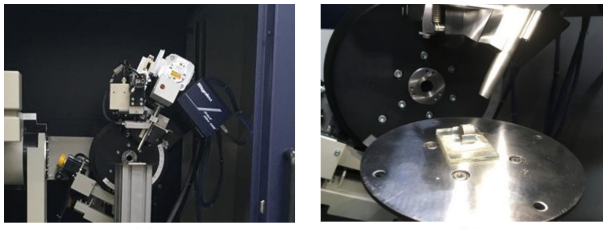

(a) (b)

Fig. 9. Measurement of the 1A sample by diffraction (a) external view of the machine, (b) measurement position

3.3. Numerical simulations

After the printing parameters setup steps according to factorial planning for each sample, it was possible to measure the thermal distortions and calculate the residual stresses. Distortions were measured at a total of 15 points distributed on the cylindrical surface, five points at the height of 2.5 mm from the base, five points at a height of 5.0 mm, and, finally, 5 points at a height of 7.5 mm sample. Figure 10 shows some of the points measured in the simulation stage. The residual stress was measured by a single point of the same coordinate considered in the experimental stage.

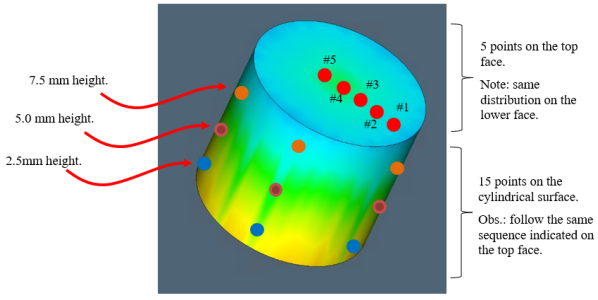

Fig. 10. Distortion measurement points simulation stage

Table 3 presents the distortion and residual stress results from the experimental stages and simulations for each of the 16 specimens, with the respective relative percentage deviations between the values obtained. Excellent approximations can be observed between the values obtained through experimental measurements and the results obtained through computer simulation.

3.4. Analysis of variance (ANOVA)

Figure 11 presents the Pareto chart with the reference line for statistical significance ($\alpha = 0.05$) for Diameter analysis. The factors and their interactions that present values lower than the reference line (to the left of the line) do not present statistical significance in the result of the studied response. The laser power and the scan speed factors showed statistical significance. The analysis result indicated that the Power and Speed factors influence the diameter of the part at a confidence level of 95%. The other combinations between the factors did not present statistical significance, at an adequate confidence level (95%), for any discussion or correlation with the response result.

In Figure 12, the interaction for the main factors that significantly correlate with the influence of Diameter, Power, and scan speed can be seen through the main effects graph. It is observed that there was a slight variation in diameter for the parameters used and that there is a tendency to increase the diameter as speed increases and Power reduces. There was an increase in the Diameter for laser power in the range of 100 W and scan speed of 1500 mm/s.

Figure 13 presents the Pareto chart with the reference line for statistical significance ($\alpha = 0.05$) for Residual stress analysis. The scan speed, the laser power, and the Hatch factors presented statistical significance at an adequate confidence level (95%).

Table 3.
Results of experimental and simulated distortions and residual stresses

Test order	Experimental diameter, mm	FEM diameter, mm	Error, %	Experimental residual sterss, MPa	FEM residual sterss, MPa	Error, %
1	11.393	11.249	1.3	294	279.3	5.0
2	11.291	11.246	0.4	135	138.2	2.4
3	11.247	11.246	0.0	133	134.1	0.8
4	11.333	11.244	0.8	124	124.7	0.6
5	11.381	11.244	1.2	70	70.4	0.6
6	11.338	11.249	0.8	143	141.8	0.8
7	11.309	11.245	0.6	100	100	0.0
8	11.361	11.246	1.0	135	141.1	4.5
9	11.481	11.243	2.1	185	176.5	4.6
10	11.322	11.249	0.6	260	246.8	5.1
11	11.36	11.246	1.0	97	96.6	0.4
12	11.44	11.246	1.7	160	160.5	0.3
13	11.22	11.251	0.3	234	218.3	6.7
14	11.205	11.248	0.4	150	150.6	0.4
15	11.335	11.244	0.8	34	36.2	6.5
16	11.302	11.245	0.5	124	123.1	0.7

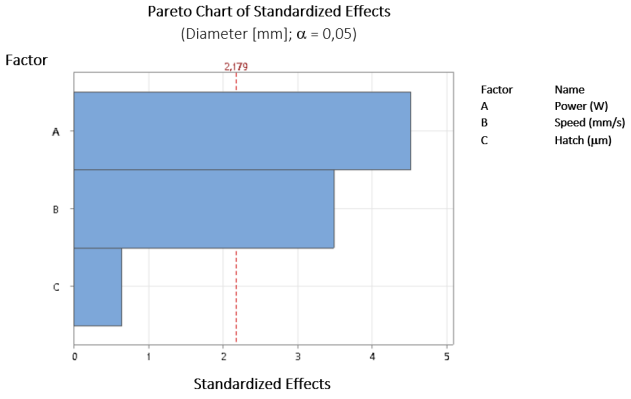

Fig. 11. Pareto chart for the diameter of the samples

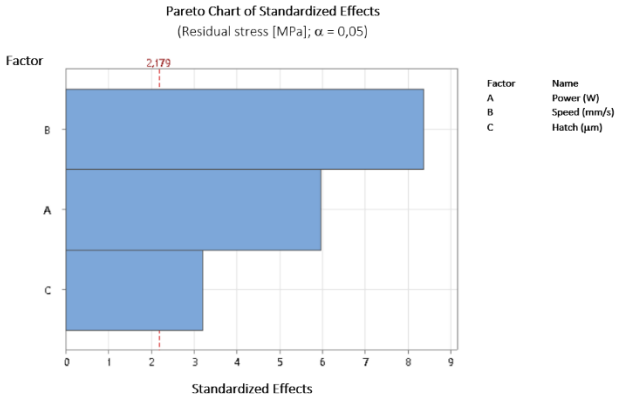

Fig. 13. Pareto chart for residual stress of 316L samples

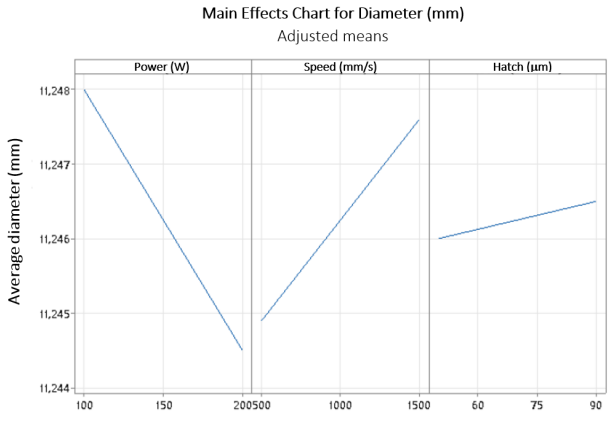

Fig. 12. Main effects chart for the diameter of the samples

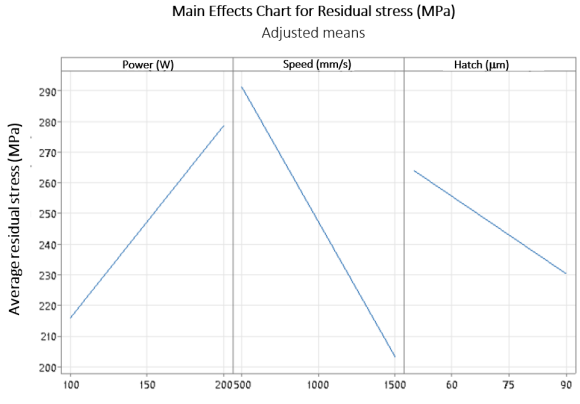

Fig. 14. Graph plot of main effects for Residual Stresses on the 316L stainless steel sample sides

Figure 14 presents the graphs of the main effects of the factors on the result of Residual stress. It can be seen that the increase in Power promoted an increase in the residual stress, while the increase in speed and hatch distance reduced the residual stress values.

4. Conclusions

After the studies, the modelling of the distortions showed good repeatability, while the residual stresses and their measurements in a single point present significant uncertainty. Thus, the software can be concluded to accurately predict the distortion and, qualitatively, the residual stresses measured on the surfaces studied.

The cooling rate and the transient thermal history are the controlling factors that significantly influence the formation of residual stresses. The factors were explored indirectly through the process parameters. It was possible to verify that laser power and scan speed also influenced the average diameter. Increasing laser power decreased the average diameter of the samples, while increasing scan speed and hatch distance increased the average diameter. When the results are compared to measure the average diameters, it is observed that the relative error was less than 2.5%, indicating an excellent correlation between the FEM predictions and the physical model measured in the experimental tests.

Laser power, scan speed, and the hatch itself greatly influenced the residual stress measured on the lateral face in the longitudinal direction of the AISI 316L steel parts. Increasing power increases residual stress, while increasing speed and the hatch decreases residual stress. When the results are compared to measure the residual stresses of the 316L samples, the maximum relative error is less than 7%; however, in most cases, the error is less than 1%, indicating a good approximation of the computational modelling to the physical model despite the high standard deviation of experimental residual stress measurements.

Research funding

The authors carried out the present research with their funding and declared that they have no known competing financial interests or personal relationships that could have appeared to influence the work reported in this paper.

Authors contribution

Authorship contribution statement: G.F. Batalha and M. O. Santos: writing review & editing, writing an original draft, methodology, investigation, formal analysis, data curation, Numerical Simulation, Conceptualization – 60%. A. Farias, E. Bordinassi, V. Seriacopi, and M Adamiak: writing review & editing, bibliographic research, statistical modelling – 40%. The authors are solely responsible for the information included in the work.

Acknowledgements

The authors acknowledge Omnitek for providing the L-PBF printing facilities, Hexagon MSC for providing the FEM software, Vtech for supporting the 3D-DIC tests, IPEN for supporting the residual stresses measurements, and USP/Maua Institute of Technology for the infrastructure.

Additional information

Selected issues related to this paper were presented at the 26th International Scientific Conference on "Achievements in Mechanical and Materials Engineering with Bioengineering and Dental Engineering" AMME & bio 2024 organised on 20th-23rd May 2024 in Wisła Malinka, Poland.

References

[1] Z. Jin, Z. Zhang, K. Demir, G.X. Gu, Machine Learning for Advanced Additive Manufacturing, Matter 3/5 (2020) 1541-1556. DOI: https://doi.org/10.1016/j.matt.2020.08.023

[2] G. Prashar, H. Vasudev, D. Bhuddhi, Additive manufacturing: expanding 3D printing horizon in industry 4.0, International Journal on Interactive Design and Manufacturing 17 (2023) 2221-2235. DOI: https://doi.org/10.1007/s12008-022-00956-4

[3] H.B. Mamo, M. Adamiak, A. Kunwar, 3D printed biomedical devices and their applications: A review on state-of-the-art technologies, existing challenges, and future perspectives, Journal of the Mechanical Behavior of Biomedical Materials 143 (2023) 105930. DOI: https://doi.org/10.1016/j.jmbbm.2023.105930

[4] M. Khorasani, J. Loy, A.H. Ghasemi, E. Sharabian, M. Leary, H. Mirafzal, P. Cochrane, B. Rolfe, I. Gibson, A review of Industry 4.0 and additive manufacturing synergy, Rapid Prototyping Journal 28/8 (2022) 1462-1475. DOI: https://doi.org/10.1108/RPJ-08-2021-0194

[5] U.M. Dilberoglu, B. Gharehpapagh, U. Yaman, M. Dolen, The Role of Additive Manufacturing in the Era of Industry 4.0, Procedia Manufacturing 11 (2017) 545-554. DOI: https://doi.org/10.1016/j.promfg.2017.07.148

[6] P. Baras, J. Sawicki, Numerical analysis of mechanical properties of 3D printed aluminium components with variable core infill values, Journal of Achievements in Materials and Manufacturing Engineering 103/1 (2020) 16-24. DOI: https://doi.org/10.5604/01.3001.0014.6912

[7] M. Deroszewska, R. Saraczyn, A. Cisowski, T. Kowaluk, T. Borowski, J. Petru, D. Myszka, Investigation of the impact of porosity of elements made using DMLS 3D printing technology and various printing angles on the mechanical properties and microstructure of 17-4 PH stainless steel, Journal of Achievements in Materials and Manufacturing Engineering 121/2 (2023) 289-305. DOI: https://doi.org/10.5604/01.3001.0054.3050

[8] E. Brancewicz-Steinmetz, J. Sawicki, Post-processing in multi-material 3D printing, Journal of Achievements in Materials and Manufacturing Engineering 117/1 (2023) 5-14. DOI: https://doi.org/10.5604/01.3001.0053.5953

[9] M. Król, L.A. Dobrzański, Ł. Reimann, I. Czaja, Surface quality in selective laser melting of metal powders, Archives of Materials Science and Engineering 60/2 (2013) 87-92.

[10] M. Król, T. Tański, Surface quality research for selective laser melting of Ti-6AL-4V alloy, Archives of Metallurgy and Materials 61/3 (2016) 1291-1296. DOI: https://doi.org/10.1515/amm-2016-0213

[11] J. Hajnys, M. Pagáč, J. Měsíček, J. Petru, M. Król, Influence of Scanning Strategy Parameters on Residual Stress in the SLM Process According to the Bridge Curvature Method for AISI 316L Stainless Steel, Materials 13/7 (2020) 1659. DOI: https://doi.org/10.3390/ma13071659

[12] E.C. Bordinassi, V. Seriacopi, M.O. dos Santos, N.W. Paschoalinoto, A. de Farias, Effect of cryogenic cooling on residual stresses and surface finish of 316L during hybrid manufacturing, The International Journal of Advanced Manufacturing Technology 129 (2023) 1489-1502. DOI: https://doi.org/10.1007/s00170-023-12380-3

[13] A.S. Wu, D.W. Bown, M. Kumar, G.F. Gallegos, W.E. King, An Experimental Investigation into Additive Manufacturing-Induced Residual Stresses in 316L Stainless Steel, Metallurgical and Materials Transactions A 45 (2014) 6260-6270. DOI: https://doi.org/10.1007/s11661-014-2549-x

[14] S. Waqar, K. Guo, J. Sun, FEM analysis of thermal and residual stress profile in selective laser melting of 316L stainless steel, Journal of Manufacturing Processes 66 (2021) 81-100. DOI: https://doi.org/10.1016/j.jmapro.2021.03.040

[15] C. Casavola, S.L. Campanelli, C. Pappalettere, Experimental analysis of residual stresses in the Selective Laser Melting process, Proceedings of the XIth International Congress and Exposition, Orlando, USA, 2008.

[16] J.H. Yu, Q.Y. Jin, K. Ha, W. Lee, Influence of Several Heat Treatments on Residual Stress in Laser Powder Bed-Fused Maraging 18Ni-300 Steel, Applied Sciences 13/11 (2023) 6572. DOI: https://doi.org/10.3390/app13116572

[17] E.C. Bordinassi, S.U. Mhurchadha, V. Seriacopi, S. Delijaicov, S.M.G. Lebrão, K. Thomas, G.F. Batalha, R. Raghavendra, Effect of hybrid manufacturing (AM-machining) on the residual stress and pitting corrosion resistance of 316L stainless steel, Journal of the Brazilian Society of Mechanical Sciences and Engineering 44 (2022) 491. DOI: https://doi.org/10.1007/s40430-022-03813-3

[18] C.E. Protasov, V.A. Safronov, D.V. Kotoban, A.V. Gusarov, Experimental study of residual stresses in metal parts obtained by selective laser melting, Physics Procedia 83 (2016) 825-832. DOI: https://doi.org/10.1016/j.phpro.2016.08.085

[19] Q.-Y. Jin, D. Kang, K. Ha, J.H. Yu, W. Lee, Simulation of annealing process on AISI 316 L stainless steel fabricated via laser powder bed fusion using finite element method with creep, Additive Manufacturing 60/A (2022) 103255. DOI: https://doi.org/10.1016/j.addma.2022.103255

[20] P. Bian, J. Shi, Y. Liu, Y. Xie, Influence of laser power and scanning strategy on residual stress distribution in additively manufactured 316L steel, Optics and Laser Technology 132 (2020) 106477. DOI: https://doi.org/10.1016/j.optlastec.2020.106477

[21] C. Kushan, M. Poyraz, Ö. Uzunonat, Y.S Orak, Systematical review on the numerical simulations of laser-powered bed additive manufacturing, Sigma Journal of Engineering and Natural Science 36/4 (2018) 1197-1214.

[22] L. Parry, I.A. Ashcroft, R.D. Wildman, Understanding the effect of laser scan strategy on residual stress in selective laser melting through thermo-mechanical simulation, Additive Manufacturing 12/A (2016) 1-15. DOI: https://doi.org/10.1016/j.addma.2016.05.014

[23] Z. Yan, W. Liu, Z. Tang, X. Liu, N. Zhang, M. Li, H. Zhang, Review on thermal analysis in laser-based additive manufacturing, Optics and Laser Technology 106 (2018) 427-441. DOI: https://doi.org/10.1016/j.optlastec.2018.04.034

[24] A. Olleak, Z. Xi, Efficient LPBF process simulation using finite element modeling with adaptive remeshing for distortions and residual stresses prediction, Manufacturing Letters 24 (2020) 140-144. DOI: https://doi.org/10.1016/j.mfglet.2020.05.002

[25] T. Kim, K. Ha, Y.R. Cho, J.B. Jeon, W. Lee, Analysis of residual stress evolution during powder bed fusion process of AISI 316L stainless steel with experiment and numerical modeling, The International Journal of Advanced Manufacturing Technology 105 (2019) 309-323. DOI: https://doi.org/10.1007/s00170-019-04204-0

[26] M.A. Mahmood, A. Ur Rehman, T. Khan, T.D. Seers, F. Liou, M. Khraisheh, Defects quantification of additively manufactured AISI 316L stainless steel parts via non-destructive analyses: Experiments and semi-FEM-analytical-based modeling, Optics and Laser Technology 174 (2024) 110684. DOI: https://doi.org/10.1016/j.optlastec.2024.110684
[27] P. Promoppatum, S.-C. Yao, Influence of scanning length and energy input on residual stress reduction in metal additive manufacturing: Numerical and experimental studies, Journal of Manufacturing Processes 49 (2020) 247-259. DOI: https://doi.org/10.1016/j.jmapro.2019.11.020
[28] L. Cheng, A. To, Part-scale build orientation optimization for minimizing residual stress and support volume for metal additive manufacturing: Theory and experimental validation, Computer-Aided Design 113 (2019) 1-23. DOI: https://doi.org/10.1016/j.cad.2019.03.004
[29] C. Li, J.F. Liu, X.Y. Fang, Y.B. Guo, Efficient predictive model of part distortion and residual stress in selective laser melting, Additive Manufacturing 17 (2017) 157-168. DOI: https://doi.org/10.1016/j.addma.2017.08.014
[30] J.L. Bartlett, B.P. Croom, J.F. Burdick, D. Henkel, X. Li, Revealing mechanisms of residual stress development in additive manufacturing via digital image correlation, Additive Manufacturing 22 (2018) 1-12. DOI: https://doi.org/10.1016/j.addma.2018.04.025
[31] R.J. Williams, F. Vecchiato, J. Kelleher, M.R. Wenman, P.A. Hooper, C.M. Davies, Effects of heat treatment on residual stresses in the laser powder bed fusion of 316L stainless steel: Finite element predictions and neutron diffraction measurements, Journal of Manufacturing Process 57 (2020) 641-653. DOI: https://doi.org/10.1016/j.jmapro.2020.07.023
[32] K. Ha, T. Kim, G.Y. Baek, J.B. Jeon, D.-s. Shim, Y.H. Moon, W. Lee, Numerical study of the effect of progressive solidification on residual stress in single-bead-on plate additive manufacturing, Additive Manufacturing 34 (2020) 101245. DOI: https://doi.org/10.1016/j.addma.2020.101245
[33] F.C. Pinto, L.S. Aota, I.R. Souza Filho, D. Raabe, H.R.Z. Sandim, Recrystallization in non-conventional microstructures of 316L stainless steel produced via laser powder-bed fusion: effect of particle coarsening kinetics, Journal of Materials Science 57/21 (2022) 9576-9598. DOI: https://doi.org/10.1007/s10853-021-06859-1
[34] E. Ramirez-Cedillo, M.J. Uddin, J.A. Sandoval-Robles, R.A. Mirshams, L. Ruiz-Huerta, C.A. Rodriguez, H.R. Siller, Process planning of L-PBF of AISI 316L for improving surface quality and relating part integrity with microstructural characteristics, Surface Coating Technology 396 (2020) 125956. DOI: https://doi.org/10.1016/j.surfcoat.2020.125956
[35] J. Yu, D. Kim, K. Ha, J.B. Jeon, W. Lee, Strong feature size dependence of tensile properties and its microstructural origin in selectively laser melted 316L stainless steel, Materials Letters 275 (2020) 128161. DOI: https://doi.org/10.1016/j.matlet.2020.128161
[36] J. Yu, D. Kim, K. Ha, J.B. Jeon, D.J. Kim, W. Lee, Size effect due to contour laser scanning in 316L stainless steel produced by laser powder bed fusion, Journal of Materials Research and Technology 15 (2021) 5554-5568. DOI: https://doi.org/10.1016/j.jmrt.2021.11.034
[37] M. Li, X. Zhang, W.-Y. Chen, T.S. Byun, Creep behavior of 316L stainless steel manufactured by laser powder bed fusion, Journal Nuclear Materials 548 (2021) 152847. DOI: https://doi.org/10.1016/j.jnucmat.2021.152847
[38] L. Cui, S. Jiang, J. Xu, R.L. Peng, R.T. Mousavian, J. Moverare, Revealing relationships between microstructure and hardening nature of additively manufactured 316L stainless steel, Materials and Design 198 (2021) 109385. DOI: https://doi.org/10.1016/j.matdes.2020.109385
[39] Q. Chen, X. Liang, D. Hayduke, J. Liu, L. Cheng, J. Oskin, R. Whitmore, A.C. To, An inherent strain based multiscale modeling framework for simulating part scale residual deformation for direct metal laser sintering, Additive Manufacturing 28 (2019) 406-418. DOI: https://doi.org/10.1016/j.addma.2019.05.021
[40] X. Song, S. Feih, W. Zhai, C.-N. Sun, F. Li, R. Maiti, J. Wei, Y. Yang, V. Oancea, L.R. Brandt, A.M. Korsunsky, Advances in additive manufacturing process simulation: Residual stresses and distortion predictions in complex metallic components, Materials and Design 193 (2020) 108779. DOI: https://doi.org/10.1016/j.matdes.2020.108779
[41] K. Carpenter, A. Tabei, On Residual Stress Development, Prevention, and Compensation in Metal Additive Manufacturing, Materials 13/2 (2020) 255. DOI: https://doi.org/10.3390/ma13020255
[42] S. Dryepondt, P. Nandwana, P. Fernandez-Zelaia, F. List, Microstructure and high temperature tensile properties of 316L fabricated by laser powder-bed fusion, Additive Manufacturing 37 (2021) 101723. DOI: https://doi.org/10.1016/j.addma.2020.101723
[43] P. Alvarez, J. Ecenarro, I. Setien, M. San Sebastian, A. Echeverria, L. Eciolaza, Computationally efficient distortion prediction in Powder Bed Fusion Additive Manufacturing. International Journal of Engineering Research and Science 2/10 (2016) 39-46.
[44] B. Cheng, S. Shrestha, K. Chou, Stress and deformation evaluations of scanning strategy effect in selective laser

melting, Additive Manufacturing 12/B (2016) 240-251. DOI: https://doi.org/10.1016/j.addma.2016.05.007
[45] A.J Dunbar, E.R. Denlinger, J. Heigel, P. Michaleris, P. Guerrier, R. Martukanitz, T.W. Simpson, Development of experimental method in situ distortion and temperature measurements during the laser powder bed fusion additive manufacturing process, Additive Manufacturing 12/A (2016) 25-30. DOI: https://doi.org/10.1016/j.addma.2016.04.007
[46] S.A. Khairallah, A. Anderson, Mesoscopic simulation model of selective laser melting of stainless-steel powder, Journal of Materials Processing Technology 214/11 (2014) 2627-2636. DOI: https://doi.org/10.1016/j.jmatprotec.2014.06.001
[47] V.A. Safronov, R.S. Khmyrov, D.V. Kotoban, A.V. Gusarov, Distortions and residual stresses at layer-by-layer additive manufacturing by fusion, Journal of Manufacturing Science and Engineering 139/3 (2017) 031017. DOI: https://doi.org/10.1115/1.4034714
[48] A.B. Spierings, N. Herres, G. Levy, Influence of the particle size distribution on surface quality and mechanical properties in additive manufactured stainless steel parts, Rapid Prototyping Journal 17/3 (2011) 195-202. DOI: https://doi.org/10.1108/13552541111124770
[49] H. Roirand, A. Pugliara, B. Malard, A. Hor, N. Saintier, Multiscale study of additively manufactured 316L microstructure sensitivity to heat treatment over a wide temperature range, Materials Characterization 208 (2024) 113603. DOI: https://doi.org/10.1016/j.matchar.2023.113603
[50] G. Mohr, S.J. Altenburg, K. Hilgenberg, Effects of inter layer time and build height on resulting properties of 316L stainless steel processed by laser powder bed fusion, Additive Manufacturing 32 (2020) 101080. DOI: https://doi.org/10.1016/j.addma.2020.101080
[51] H. Sohrabpoor, V. Salarvand, R. Lupoi, Q. Chu, W. Li, B. Aldwell, W. Stanley, S. O'Halloran, R. Raghavendra, C.-H. Choi, D. Brabazon, Microstructural and mechanical evaluation of post-processed SS 316L manufactured by laser-based powder bed fusion, Journal of Materials Research and Technology 12 (2021) 210-220. DOI: https://doi.org/10.1016/j.jmrt.2021.02.090
[52] Z. Zheng, L. Peng, D. Wang, Defect Analysis of 316 L Stainless Steel Prepared by LPBF Additive Manufacturing Processes, Coatings 11/12 (2021) 1562. DOI: https://doi.org/10.3390/coatings11121562
[53] D. Cortis, D. Pilone, G. Broggiato, G.F. Campana, D. Tatananni, D. Orlandi, Setting of L-PBF parameters for obtaining high density and mechanical performance of AISI 316L and 16MnCr5 alloys with fine laser spot size, Progress in Additive Manufacturing (2023). DOI: https://doi.org/10.1007/s40964-023-00556-y
[54] S. Cacace, L. Pagani, B.M. Colosimo, Q. Semeraro, The effect of energy density and porosity structure on tensile properties of 316L stainless steel produced by laser powder bed fusion, Progress in Additive Manufacturing 7 (2022) 1053-1070. DOI: https://doi.org/10.1007/s40964-022-00281-y
[55] M.A. Chaudry, G. Mohr, K. Hilgenberg, Experimental and numerical comparison of heat accumulation during laser powder bed fusion of 316L stainless steel, Progress in Additive Manufacturing 7 (2022) 1071-1083. DOI: https://doi.org/10.1007/s40964-022-00282-x
[56] X. Yan, J. Pang, Y. Jing, Ultrasonic Measurement of Stress in SLM 316L Stainless Steel Forming Parts Manufactured Using Different Scanning Strategies, Materials 12/17 (2019) 2719. DOI: https://doi.org/10.3390/ma12172719
[57] ASTM F3184-16, Additive Manufacturing Stainless Steel Alloy (UNS S31603) with Powder Bed Fusion, ASTM International, West Conshohocken, PA, 2024. DOI: https://doi.org/10.1520/F3184-16
[58] Carpenter Technology Corporation, PowderRange 316L Datasheet. Available from: https://www.carpenteradditive.com/hubfs/Resources/Data%20Sheets/PowderRange_316L_Datasheet.pdf (Access in: 15.06.2024)